An Integrated Overview of CAD/CAE Tools and Their Use on Wireless Communication Circuits Design

José Carlos Pedro and Nuno Borges Carvalho

e-mail: jcpedro@ieee.org and nborges@ieee.org
Instituto de Telecomunicações – Universidade de Aveiro, 3810 AVEIRO – Portugal

Shortened title: "Overview of Wireless Circuits' CAD Tools"

Keywords: RF Circuit Simulation, Nonlinear Modelling, Design Validation, RF Power Amplifier

Abstract — An integrated overview of CAD/CAE tools for nonlinear circuits design is presented, bridging the existing gaps between simulation algorithms, modeling strategies and laboratory characterization procedures. The paper reviews the most important RF circuit analysis techniques, the mathematical circuits' and devices' representation, and discusses important design validation aspects.

I. INTRODUCTION

Nonlinear circuit analysis is nowadays a field of strong scientific intervention that spans from signal and circuit modeling, to simulation, and design validation.

Beginning with signal modeling, communication signals can be viewed as essentially narrowband information signals modulating radio frequency carriers [1]. Therefore, they ask for aperiodic stochastic descriptions involving two or more time scales. Signal representation is thus a problem of primary concern as the common approaches using CW, two-tones or even multi-tones are only different levels of simplification.

In the circuit analysis arena, the nowadays standard nonlinear RF and microwave circuit simulator tool is the harmonic-balance technique, HB [2], treating the nonlinear elements in time-domain, while the linear sub-network is handled in the frequency-domain [3]. Suffering from the need to commute between domains, HB is conditioned by the discrete Fourier transform, DFT, limitations and is thus restricted to

periodic, or, at most, quasi-periodic, signals [4]. So, although it is quite popular for simulating circuits driven by stereotype forcing functions as single-tone or two-tones, it has been difficult to apply to real telecommunication signals.

This created a renewed interest for time-domain transient methods and led to the emergence of multi-rate techniques operating in a true mixed time-frequency domain [5-10]. Treating the aperiodic information envelope as a time-varying signal modulating the frequency-domain circuit's behavior to the periodic RF carrier, these new approaches convert the original ODE into another multi-rate partial differential equation of time-varying Fourier coefficients.

In what the model development phase is concerned, this refers to a wise choice between an accurate, but restricted in application range, local model formulation, and a more approximate, but also wider, global model expression [11]. And, in the extraction phase, it demands for an appropriate balance between the use of physical and behavioral (measurement) information [11].

Finally, at the end of the design process, the real system should be measured under some wisely designed stimulus and these laboratory observations used to validate similar simulation results.

Although it is widely recognized that these various aspects play their own specific but interrelated role in the microwave and wireless circuit design process, their heterogeneity has led to separate treatments. Therefore, the main goal of this paper is to bridge the gaps between these different scientific fields giving an integrated overview of their role and importance in the complete RF circuit design process. For that, it begins by reviewing the available simulation technologies, focusing on their comparative advantages for each particular application. Then, it proposes a nonlinear circuit and device model formulation and extraction procedure, closing with the discussion of appropriate design validation methodologies.

II. Nonlinear RF Circuit Simulation Techniques

In order to get a common framework for the presentation of the various RF circuit simulation algorithms, consider the simple nonlinear network depicted in figure Fig. 1.

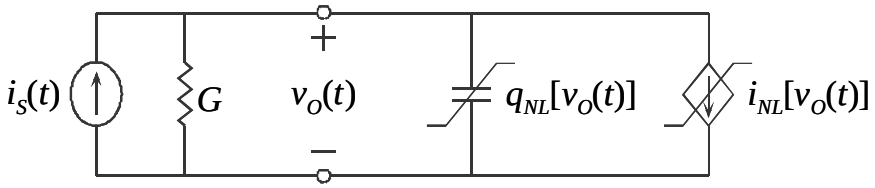

Fig. 1 – Nonlinear dynamic circuit example.

Under nodal current analysis, this circuit can be represented by the following ordinary differential equation, ODE, in time:

$$G\,v_O(t)+\frac{\mathbf{d}\,q_{NL}[v_O(t)]}{\mathbf{d}\,t}+i_{NL}[v_O(t)]=i_S(t) \tag{1}$$

To solve this ODE, several algorithms can be used like time-step integration, time-domain calculation of steady-state responses (Shooting – Newton), Frequency-Domain Methods (Harmonic-Balance or Volterra Series) and Multi-Rate Techniques. A brief presentation of these algorithms will now be presented.

Time-Step Integration

Time-step integration (also known as time-marching [12]) methods solve the circuit's ODE for $v_O(t)$ transforming it into a difference equation. For that, continuous time is discretized in various instants t_k separated by dynamic time-steps h_k which converts (1) into a nonlinear difference equation. This equation is then solved in a time-sep by time-step basis, for all $v_O(t_k)$, beginning with some predefined initial state $v_O(t_0)$ until the desired final time $v_O(t_K)$ is reached.

Since time-step integration was conceived for transient response calculations, its direct application to the RF steady-state response becomes very inefficient, requiring that we wait until all transients have died [6]. It is also inadequate since it works in time-domain while most signal and circuit models are represented in frequency-domain. Finally, it is also inaccurate because the use of the DFT requires interpolation and re-sampling between the non-uniform dynamic time-steps, and also because of the need for the ideal complete vanishing of all transients [6].

Nevertheless, time-step integration is still one of the mostly used methods of nonlinear circuit and system simulation. It is the core method of all SPICE-like circuit [12], or Simulink system [13] simulation programs.

Time-Domain Calculation of Steady-State Periodic Responses (Shooting – Newton)

In order to overcome some of the above disadvantages associated with time-step integration, shooting methods calculate directly the steady-state response in time-domain. They bypass the transient computation selecting a certain initial condition, $v_O(t_0)$, such that, after the excitation period, T, the same initial state is obtained [6]:

$$v_O(t_0+T) = v_O(t_0) \quad \text{for} \quad i_S(t_0+T) = i_S(t_0) \tag{2}$$

The underlying idea consists in evaluating the sensitivity of the final state, $v_O(t_0+T)$, to variations in the initial condition, $v_O(t_0)$:

$$S[v_O(t_0)] \equiv \left.\frac{\partial v_O(t_0+T)}{\partial v_O(t_0)}\right|_{v_O(t_0)} \approx \frac{\Delta v_O(t_0+T)}{\Delta v_O(t_0)} \tag{3}$$

and then use this sensitivity to propose an educated guess for the correct initial condition $v_O(t_0)$ [14]. That is, this method converts the nonlinear transient initial value problem of (1) into the new nonlinear periodic boundary value problem of (2), which is then solved for $v_O(t_0) = v_O(t_0+T)$ using a Newton-Raphson iteration scheme. Known as the Shooting-Newton [14], it constitutes a serious alternative for RF steady-state simulation since $S[^i v_O(t_0)]$ can be obtained along with time-step integration without the need for any additional post-processing, and because it has been verified that the boundary-value equation $v_O(t_0+T)-v_O(t_0)=0$ is usually mildly nonlinear, despite the circuit may be pushed well into strongly nonlinear regimes [6].

Frequency Domain Methods

The conventional RF approach to solve our original nonlinear ODE, takes profit of the special property of Fourier expansions in converting differential equations into much simpler algebraic formulations. In this way, the objective ceases to be a set of output instants, but a vector of coefficients of the Fourier expansion. So, both the excitation and the state-variables are represented as truncated Fourier series:

$$i_S(t) = \sum_{k=-K}^{K} I_{s_k}\, \mathbf{e}^{jk\omega_0 t} \quad \text{and} \quad v_O(t) = \sum_{k=-K}^{K} V_{o_k}\, \mathbf{e}^{jk\omega_0 t} \tag{4}$$

which, substituted in the circuit's time-domain ODE, of (1) leads to a nonlinear system of (2*K*+1) equations, one for each harmonic component *k*. In matrix form, this system is known as the Harmonic-Balance Equation:

$$G\,\mathbf{V}_o + j\boldsymbol{\Omega}\mathbf{Q}_{nl}(\mathbf{V}_o) + \mathbf{I}_{nl}(\mathbf{V}_o) - \mathbf{I}_s = 0 \tag{5}$$

There are two possible ways of solving this HB equation: the Volterra Series and the Harmonic-Newton.

In the Volterra series it is assumed that (5) is only mildly nonlinear, so that its solution can be approximated by the analytical solution of a similar problem in which the nonlinearities are locally approximated by low order Taylor series expansions around some pre-defined quiescent point [11,15,16]. The solution can then be expressed in the frequency-domain by [11]:

$$v_o(t) = \sum_{n=1}^{\infty} \frac{1}{2^n} \sum_{q_1=-Q}^{Q} \cdots \sum_{q_n=-Q}^{Q} I_{Sq_1} \cdots I_{Sq_n}\, H_n(\omega_{q_1}, \cdots, \omega_{q_n})\, e^{j(\omega_{q_1}+\cdots+\omega_{q_n})t} \tag{6}$$

which states that, expanded in a Volterra series, the system becomes completely identified by its *n*'th order Nonlinear Transfer Functions, NLTFs, $H_n(\omega_1,\ldots,\omega_n)$ [11, 15, 16, 17]. Being a true analytical model of a nonlinear dynamic system, the main advantage of Volterra series is its ability to provide qualitative information, and thus being amenable for circuit design.

It is known that most mildly RF nonlinear circuits can be described with enough accuracy by a 3rd order Volterra series. However, the conditions describing this "mildly nonlinear" behavior are not clear. Actually, Volterra series suffer from a limited range of convergence (they require smooth behavior of the nonlinear function and its derivatives in the whole domain of signal amplitude and memory span [16]), but also from the eventual necessity of an intractable number of NLTFs. In fact, practical observations have shown that the Volterra formulation has its usefulness normally restricted to excitation amplitudes much smaller that the quiescent point, for example, comfortably below the circuit's 1dB compression point [11].

Alternatively, the full nonlinear harmonic-balance equation of (5) can be numerically solved for V_o using a (2K+1) dimensional Newton-Raphson algorithm. This harmonic-Newton simulation engine is clearly the most used method for microwave circuit simulation. In its most common implementation - piecewise harmonic-Newton [3] - the network is divided into two sub-circuits as shown in Figure 2. One of these sub-circuits is nonlinear and memoryless, while the other is dynamic but necessarily linear. By adding the excitation, this allows the construction of a nodal form of the HB equation:

$$\mathbf{F}(\mathbf{V}_o) \equiv I_{cl}(\mathbf{V}_o) + I_{cnl}(\mathbf{V}_o) - I_s(\omega) = 0 \tag{7}$$

where $I_{cl}(\mathbf{V}_o) = Y_{cl}(\omega)V_o(\omega)$ and $I_{cnl}(\mathbf{V}_o) = DFT\{i_{CNL}[DFT^{-1}[V_o(\omega)]]\}$.

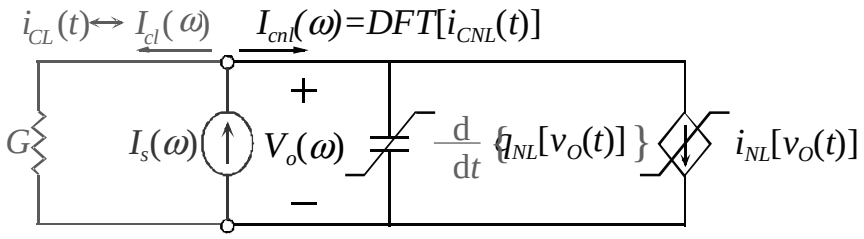

Fig. 2 – Division of the circuit into a nonlinear and a linear sub-networks according to the piecewise HB implementation.

The conventional harmonic-Newton, or some of its newer implementations using quasi-Newton techniques [18], has been successfully applied to a large variety of microwave nonlinear circuits like amplifiers [19] mixers [20] and oscillators [21]. Relying on iterative methods for solving the associated Newton-Raphson linear system [22], they have recently relaxed the necessity of handling large Jacobian matrices, allowing their application to circuits (or systems) involving a huge number of unknowns [18].

Nevertheless, the necessity of passing from the time to frequency-domain, and vice-versa, requires the use of the DFT, and so restricts HB application to stimuli and responses where this signal processing tool is both valid and efficient. Therefore, this traditional form of HB leaves outside true non-commensurate multi-tone (quasi-periodic or aperiodic) signals [11] and strong nonlinear regimes where the DFT demands for a very large number of coefficients [11].

Multi-Rate Techniques

Multi-rate techniques appeared exactly to ease the difficulties in handling quasi-periodic signals [5, 23], and have gained a strong acceptance in the wireless circuit design area because of the typical two time-rate nature of these modulated RF signals.

When the excitation is an RF carrier $\cos(\omega_0 t)$ modulated by a base-band envelope $v_e(t)$, which is uncorrelated with the carrier, the circuit behaves as if it had a stimulus dependent on two different time-scales τ_1 and τ_2:

$$i_S(\tau_1,\tau_2) = V_e(\tau_1)\cos(\omega_0\tau_2) \tag{8}$$

The original circuit's ODE, in t shown in (1) becomes a Multi-Rate Partial Differential Equation, MPDE, in (τ_1,τ_2) [5, 9]:

$$G\,v_O(\tau_1,\tau_2) + \frac{\partial\, q_{NL}\left[v_O(\tau_1,\tau_2)\right]}{\partial\,\tau_1} + \frac{\partial\, q_{NL}\left[v_O(\tau_1,\tau_2)\right]}{\partial\,\tau_2} + i_{NL}\left[v_O(\tau_1,\tau_2)\right] = i_S(\tau_1,\tau_2) \tag{9}$$

which can now be solved in a bi-dimensional time-domain for $v_O(\tau_1, \tau_2)$, or bi-dimensional frequency-domain for $V_o(k_1\Omega_0, k_2\omega_0)$, whether transient or doubly-periodic responses are desired [5, 9].

If both the envelope and the carrier are periodic and the consequent doubly-periodic regime is sought, it is better to solve the MPDE in a bi-dimensional frequency-domain. In this case, the state variable would be described by:

$$v_O(\tau_1, \tau_2) = \sum_{k_1} \sum_{k_2} V_{k_1,k_2} e^{jk_1\Omega_0\tau_1} e^{jk_2\omega_0\tau_2} \tag{10}$$

which substituted in the MPDE leads to the following bi-dimensional HB equation, the basis for most of the multi-tone nonlinear simulation methods [4]:

$$G.\mathbf{V}_o(\Omega, \omega) + \mathbf{I}_{nl}[\mathbf{V}_o(\Omega, \omega)] + j\boldsymbol{\Omega}\, \mathbf{Q}_{nl}[\mathbf{V}_o(\Omega, \omega)] + \mathbf{I}_s(\Omega, \omega) = 0 \tag{11}$$

In most practical cases, however, the information nature of the envelope makes it an aperiodic signal, and so it is better to solve the MPDE in the frequency-domain for the carrier, ω, but in the time-domain, τ_1, for the envelope. In this case, the state variable description becomes a DFT (for the carrier) with τ_1 time varying (according to the envelope) coefficients:

$$v_O(\tau_1, \tau_2) = \sum_{k_2} V_{k_2}(\tau_1) e^{jk_2\omega_0\tau_2} \tag{12}$$

which substituted in the MPDE leads to the following τ_1 time-varying HB equation:

$$G\,\mathbf{V}_o(\tau_1) + \frac{\partial\, \mathbf{Q}_{nl}[\mathbf{V}_o(\tau_1)]}{\partial\, \tau_1} + j\boldsymbol{\Omega}\,\mathbf{Q}_{nl}[\mathbf{V}_o(\tau_1)] + \mathbf{I}_{nl}[\mathbf{V}_o(\tau_1)] - \mathbf{I}_s(\tau_1) = 0 \tag{13}$$

This time-varying HB equation can now be discretized in τ_1 time-steps, h_k, which allows the determination of the envelope transient solution for each of the $V_{ok}(\tau_1)$ harmonics.

This method, from which a particular approximate implementation is known as the Envelope Transient Harmonic-Balance [7, 8, 10], constitutes a serious step towards a true nonlinear envelope driven system simulator.

III. Nonlinear Device and Circuit Modeling

If it sounds intuitive that the model must constitute an accurate mathematical representation of the circuit's voltage and current relationships, it is no longer so obvious what metrics should be used to qualify a particular model. For achieving that goal, it is convenient to recall the Volterra expansion expressed by (6). This is a series involving two essentially different, but interrelated, entities: nonlinearity and memory.

The first one is expressed by the expansion order, *n*. Higher orders imply more complex behaviors, and so an increasing number of different responses. These add up at the output turning model identification a very difficult task.

Another aspect to take into consideration when dealing with nonlinear modeling is local and global models.

Local models are very accurate current/voltage, I/V, or charge/voltage, Q/V, representations valid only in the vicinity of a particular quiescent point [11]. Locally approximating the function and its higher order derivatives, these models achieve the best level of representation detail, guaranteeing predictive capabilities of higher order distortion effects. However, their Taylor series form [11] also indicate that they are prone to abrupt degradation when the input signal amplitude leaves the vanishing small-signal zone.

Global models, on the other hand, do not try to get an optimum representation in the vicinity of the quiescent point, but seek for an overall reasonable approximation in the whole range of excitation amplitudes [11]. This way, they usually provide a better large-signal approximation, when compared to local models, at the expense of generally worst accuracy under small-signal regimes.

One possible way to fulfill this compromise, obtaining global models still with good small signal accuracy, is to use physical device information during model development. Examples of physical based models already exist for a long time for Schottky diodes [24] and bipolar devices [25], but physical-behavioral combinations have also been proposed for GaAs MESFETs [26] and MOSFETs [27], for example.

In summary, the basic memoryless nonlinear modeling idea should be to start with a behavioral formulation selected from the knowledge of the physical operation of the device (global modeling), and then extract its model parameters from higher order characteristics obtained for different bias points under small signal operation (envisaging local accuracy). For a general bi-dimensional I/V model in which the input and output terminal currents, i_1 and i_2, depend on the input and output terminal voltages, v_1 and v_2:

$$i_1(v_1,v_2) = I_{1DC} + a_{1,10}\,v_1 + a_{1,01}\,v_2 + a_{1,20}\,{v_1}^2 + a_{1,11}\,v_1 v_2 + a_{1,02}\,{v_2}^2 + \\ + a_{1,30}\,{v_1}^3 + a_{1,21}\,{v_1}^2 v_2 + a_{1,12}\,v_1 {v_2}^2 + a_{1,03}\,{v_2}^3 + \ldots \tag{14}$$

$$i_2(v_1,v_2) = I_{2DC} + a_{2,10}\,v_1 + a_{2,01}\,v_2 + a_{2,20}\,{v_1}^2 + a_{2,11}\,v_1 v_2 + a_{2,02}\,{v_2}^2 + \\ + a_{2,30}\,{v_1}^3 + a_{2,21}\,{v_1}^2 v_2 + a_{2,12}\,v_1 {v_2}^2 + a_{2,03}\,{v_2}^3 + \ldots \tag{15}$$

these coefficients can be extracted with the set-up of Fig. 3 [26].

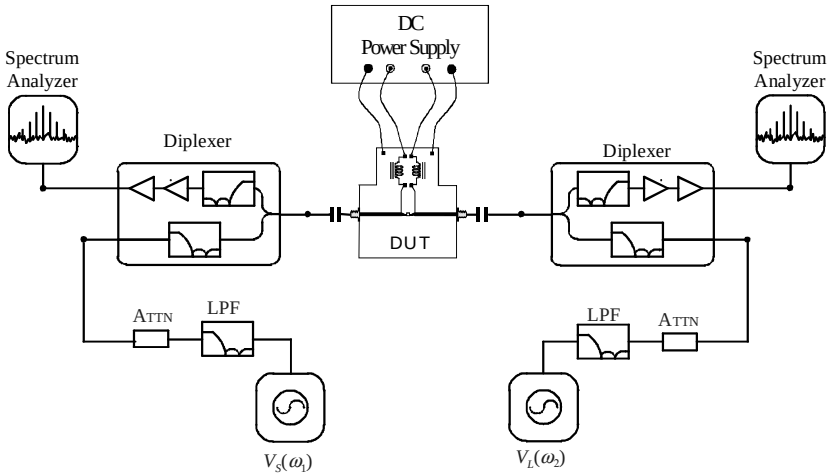

Fig. 3 – Double-input double-output local nonlinear model extraction set-up.

Turning now our attention to memory span, it presents, at least, two distinct aspects. Beginning with linear memory, i.e. memory effects associated with the first order Volterra kernel or transfer function, memory span is simultaneously a measure of impulse response length, or of required frequency resolution. It is, thus, a quantitative measure of the smoothness of $H_1(\omega)$.

When memory associated with higher order NLTFs is considered, the problem becomes much more involved. First of all, this form of memory can only be felt when the system is excited by two or more frequency components (actually a number of independent frequency components equal to the nonlinear order of the NLTF in study). Second, it may also be observed that the system can significantly change its dynamic behavior when the input amplitude is varied. For example, it may be almost memoryless under small signal regime (absence of linear memory), and then become dynamic under large signal, i.e. in presence of a strong demodulated base-band or any harmonic components. Therefore, since the complete identification of a *n*'th order NLTF requires an excitation composed by *n* different, and non interacting tones, (*n* degrees of freedom) [28], or (*n*-1) different tone separations, nonlinear memory can not be captured under CW excitation. Furthermore, since this form of memory is intrinsically mixed with nonlinearity, its extraction also demands for a wide range of excitation amplitudes.

In circuit terms, this means we need to excite all the system's dynamic states, from the fundamental zone to all of its harmonics and the base-band, even if we were only interested in the first zone output, as in band-pass telecommunications systems [1]. In wireless circuits driven by modulated signals, for instance, it has been observed that the base-band dynamics play a determinant role in accurately predicting nonlinear distortion effects [29-32].

Currently, there is an important debate on how to observe and extract nonlinear memory in general nonlinear dynamic systems. Early works of Lee and Schetzen [16] proposed time-domain measures of input-output cross-correlation when the nonlinear dynamic system is excited by Gaussian noise. Chua and his co-workers preferred frequency-domain observations using a carefully selected set of harmonically related sines and measuring the power and phase of the corresponding harmonic output components [33-

35]. Nowadays, various researchers are trying a frequency-domain extraction with deterministic or random multisines [36-38], while some others are investing in a time-domain [39-40] or mixed time-frequency [41] extraction using complex modulated signals.

Fortunately, it seems that the problem of nonlinear dynamic modeling of circuits and devices can be much simpler than this general case. If we take profit of the equivalent circuit model format and the quasi-static approximation required for all commercial HB or time-step integration solvers, we can separate memory from nonlinearity. Since these models always assume that the nonlinearities are memoryless and the dynamic elements are linear (note that even dynamic nonlinear capacitors and inductors are modeled as memoryless charges and fluxes followed by a linear differential operator to calculate terminal currents or voltages) the dynamic model extraction can always be divided into a linear de-embedding process followed by a memoryless nonlinear extraction.

That is the concept depicted in figure Fig. 4, in which, following a behavioral modeling perspective, it is assumed that the input and output bias networks do not constitute any additional excitation ports, but were embedded into the circuit.

So, considering the circuit of Fig. 4 modeled as an extrinsic nonlinear dynamic two-port defined by:

$$[i_1(t), i_2(t)] = f_{NL_{12}}\left[v_1(t), \frac{d\,v_1(t)}{d\,t}, \ldots, \frac{d^{n_1}\,v_1(t)}{d\,t^{n_1}}, v_2(t), \frac{d\,v_2(t)}{d\,t}, \ldots, \frac{d^{n_2}\,v_2(t)}{d\,t^{n_2}}\right] \tag{16}$$

and

$$\begin{cases} Z_S(\omega) I_1(\omega) + V_1(\omega) - V_S(\omega) = 0 \\ Z_L(\omega) I_2(\omega) + V_2(\omega) - V_L(\omega) = 0 \end{cases} \tag{17}$$

in which, typically, $V_L(\omega) = 0$, this same circuit can also be described by a two-port memoryless nonlinearity:

$$[i_3(t), i_4(t)] = f_{NL_{34}}[v_3(t), v_4(t)] \tag{18}$$

embedded in a four-port linear network described in the frequency-domain by its admittance matrix.

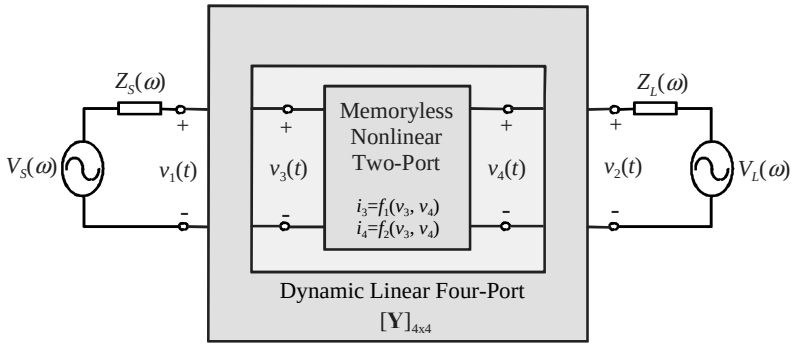

Fig. 4 – Separation of the circuit's memoryless nonlinearities from the embedding linear network.

Assuming that physical knowledge of the system in question can provide us with the embedding linear dynamic four-port topology, its 4x4 $Y_{ij}(\omega)$ parameters can then be obtained from any conventional equivalent circuit extraction technique [42]. Knowing the topology and the element values of that four-port, leads us to the relation between the extrinsic access variables [$i_1(t)$, $i_2(t)$] and [$v_1(t)$, $v_2(t)$] and the intrinsic [$i_3(t)$, $i_4(t)$] and [$v_3(t)$, $v_4(t)$], which play the role of the intrinsic nonlinearity current responses and control voltages. So, being now de-embedded from memory, this bi-dimensional memoryless nonlinearity can again be extracted using the set-up presented in Fig. 3.

For illustrating this modeling strategy with a practical example, we took the medium power amplifier circuit of figure Fig. 5, and proceeded to the extraction of a model of its embedding linear dynamic circuit and the GaAs MESFET most important nonlinearities.

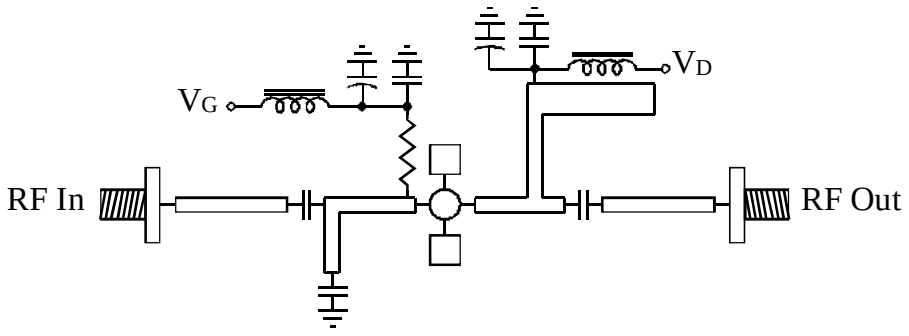

Fig. 5 – Illustrative example of a medium power amplifier circuit for nonlinear dynamic model extraction.

Since we had the actual circuit, the linear sub-network topology was directly obtained by inspection. Two different linear blocks corresponding to the input and output matching and bias networks were distinguished. After augmenting these sub-networks with the corresponding active device parasitics they were then lumped into two S-parameter matrices. As seen from the Volterra or the HB methods, these [S] matrices should have a frequency resolution corresponding to all the possible beat products of the input excitation tones. So, assuming the amplifier is to be analyzed for a RF modulated signal represented by the following multi-tone:

$$v_S(t) = \sum_{q=0}^{Q} V_{s_q}\, e^{j\left[(\omega_0 + q\Delta\omega)t + \phi_q\right]} \tag{19}$$

the output response would be described by:

$$v_O(t) = \sum_{k=0}^{K} \sum_{q_k=0}^{Q_k} V_{oq_k}\, e^{j\left[(k\omega_0 + q_k\Delta\omega)t + \phi_{q_k}\right]} \tag{20}$$

in which the output mixing products are composed by clusters of (Q_k+1) frequency components located at each of the ω_0 harmonics ($k\omega_0$) and the base-band ($0\omega_0$ or DC).

Particular attention should be paid to the accurate modeling of the embedding impedances at the various harmonics (mainly the 2nd, in a PA) and the base-band, as they might have a primary importance on the first zone output characteristics (signal output power, power added efficiency and in-band nonlinear distortion) [11]. In this respect, it is convenient to stress that, most of the times, the band-pass characteristics of the input and output matching networks obviate any attempt to evaluate these impedances looking only at the available circuit ports, and the circuit must be broken into several parts.

Furthermore, if we realize that, for example, a modern wireless signal can have bandwidths varying from some hundreds of kHz to a few MHz, while most microwave vector network analyzers have its minimum measurement frequency at some tens of MHz, added difficulties should be expected to

accurately characterize the base-band terminating impedances. Moreover, since the circuit's base-band nonlinear characteristics can be determined by the matching networks quality factor, but also by the bias networks, it should cause no surprise that smooth microwave impedances, like the ones presented in figure Fig. 6 for the output matching network near DC, can cover up complex behaviors for the base-band, as shown in Fig. 7.

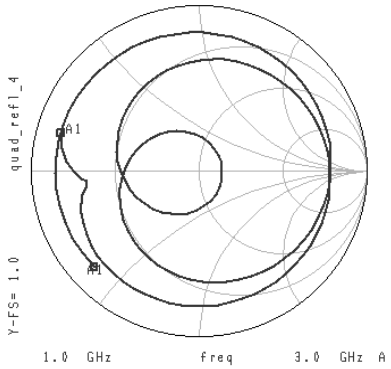

Fig. 6 – Output terminating impedance behavior in the microwave range.

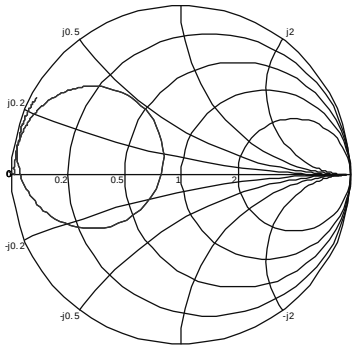

Fig. 7 – Output terminating impedance behavior for the base-band, near DC (from 10KHz to 200MHz).

After having the model for the linear embedding network, the GaAs MESFET gate-source charge, $q_{gs}(v_{GS})$ [or capacitance $C_{gs}(v_{GS})$], and channel current, $i_{DS}(v_{GS},v_{DS})$, memoryless nonlinearities were then represented using the model of [43-44]:

$$i_{DS}(v_{GS}, v_{DS}) = \beta\left[u + \ln\left(e^{u} + e^{-u}\right)\right]\tanh\left(\alpha v_{DS}\right) \tag{21}$$

$$C_{GS}(v_{GS}) = C_{GSF} + C_{GS0}[1+\tanh(u)] \tag{22}$$

where u represents a measure of active channel height and is thus dependent on gate-source voltage, v_{GS}, (but also accounts for the threshold variation with applied drain-source voltage, v_{DS}) and α, β, C_{GSF} and C_{GS0} are simply scaling empirical parameters.

Due to their physics based nature, these functions are valid in a wide range of control voltages, v_{GS} and v_{DS} (i.e., they constitute a global model), are continuous and present continuous derivatives, that approximate reasonably well the measurements at least up to the 3rd derivative (accurate local representation). They are thus consistent with measured (0 order) DC bias, (1st order) S-pararameters, and (2nd and 3rd order) harmonic and intermodulation distortion.

$i_{DS}(v_{GS},v_{DS})$ nonlinear model parameters were extracted by comparing measured I_{DS}, and all its first nine derivatives up to order 3 with respect to v_{GS} and v_{DS},

$$\begin{aligned} i_{DS}(v_{GS},v_{DS}) \approx I_{DS} + G_m v_{gs} + G_{ds} v_{ds} + G_{m2} {v_{gs}}^2 + G_{md} v_{gs} v_{ds} + G_{d2} {v_{ds}}^2 + \\ + G_{m3} {v_{gs}}^3 + G_{m2d} {v_{gs}}^2 v_{ds} + G_{md2} v_{gs} {v_{ds}}^2 + G_{d3} {v_{ds}}^3 \end{aligned} \tag{23}$$

with the ones predicted by the adopted functional description. The derivatives' extraction procedure was based on intermodulation measurements using the set-up of Fig. 3, when the device is excited at its input and output by one tone at ω_1, and another at ω_2, in the VHF range, and the response measured at the output.

As seen in figures Fig. 8 a) and b), $i_{DS}(v_{GS})$ derivatives predicted by the model are in very good agreement with correspondent measured data.

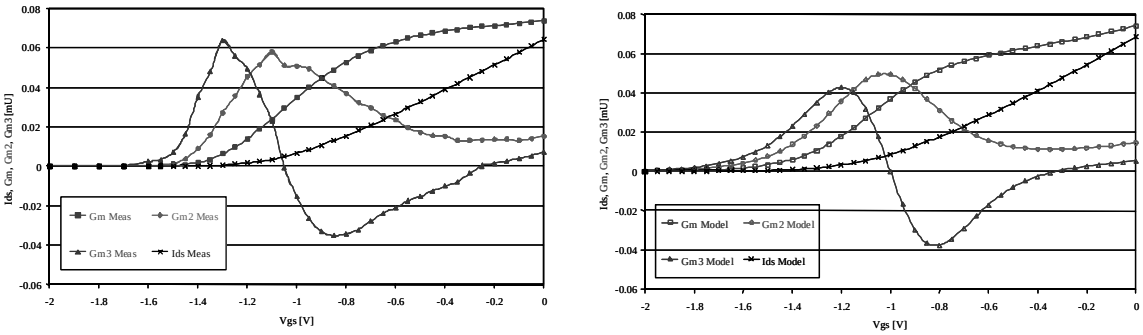

a) b)

Fig. 8 – Measured - a) and modeled - b) channel current, $i_{DS}(v_{GS})$ and its derivatives, G_m, G_{m2} and G_{m3}.

The same set-up can also be used for extracting $C_{gs}(v_{GS})$ coefficients [45], but now higher frequencies must be applied, and only the input excitation and measurement are used.

As seen in figure Fig. 9 a) and b), $C_{gs}(v_{GS})$ and its derivatives predicted by the model are again in a reasonable good agreement with correspondent measured data.

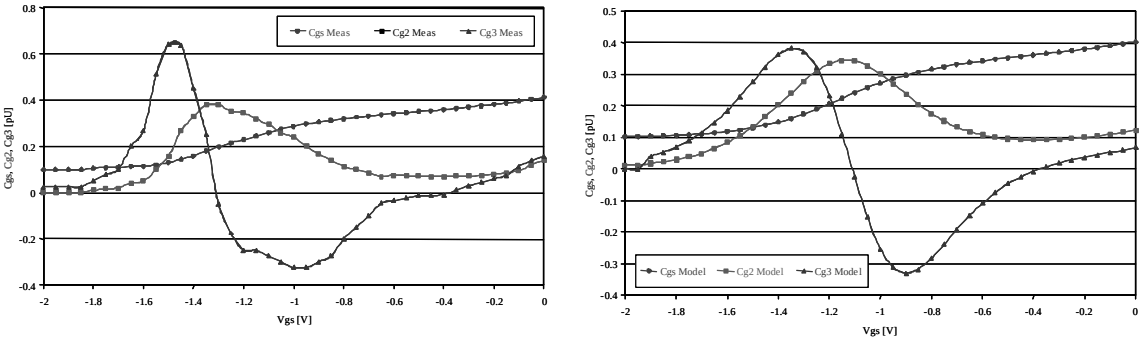

a) b)

Fig. 9 – Measured - a) and modeled - b) gate-source capacitance, $C_{gs}(v_{GS})$ and its derivatives, C_{g2} and C_{g3}.

IV. DESIGN VALIDATION

Since, in this context, design validation is a group of actions taken to confront simulation results with real measurements, its basic step consists on the selection of an appropriate set of experiments capable of providing meaningful design tests. In circuits specially conceived for particular commercial or military

applications, these experiments try to mimic the circuit's real operation, and the validation tests end up in the verification of a certain set of pre-determined specs. In general purpose circuits, these tests must have a broader applicability and be directed to a wider range of operating regimes.

Although commercial simulators are now increasing their range of excitation templates to cover most of the wireless signal standards, band-pass approximations must be used in all the missing cases. These can be synthesized in either time or frequency-domains.

In the former, more usual in the complex envelope system level simulators [13, 46, 47], several realizations of a pseudo-random bit sequence modulate an RF carrier according to the real system's modulation scheme. Then, the circuit responses are averaged over these realizations.

In frequency-domain, a discretized approximation of the real signal's power spectral density function can be built from a set of deterministic multisine realizations, as the one given by (19) [11, 36]. Then, their results are again averaged.

The circuit's response to each of these multi-tone realizations is given by (20) and takes the aspect of a series of frequency component clusters, as shown in figure Fig. 10.

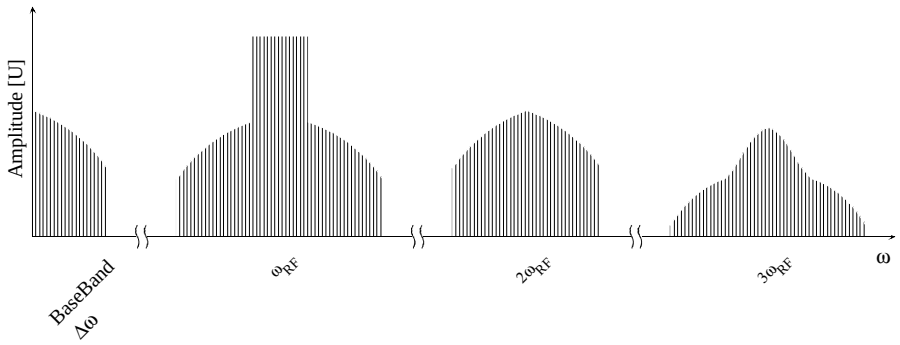

Fig. 10 –Typical circuit's response spectrum to a deterministic band-pass multisine.

Despite being simple in concept, this procedure hides some issues worth to discuss.

First, we should realize that the only essential difference between the time and frequency-domain approaches is that the former allows a true aperiodic (transient) simulation while the latter is always

assuming periodic regimes. But, it should be also noted that, in practice, not only a pseudo-random sequence is actually periodic, as every time a signal is converted to frequency-domain, it is the Fourier spectrum of a periodic signal, whose period is the simulated time-window, that is really being calculated.

The second aspect to be considered in this type of signal synthesis is the actual amplitude and phase distribution of the set of deterministic multi-tones. If the tone amplitudes, V_{s_q}, can be simply kept constant from realization to realization, and selected according to the signal's power spectral density function, the choice of phases, ϕ_q, is significantly more delicate. In fact, the example of Fig. 11, which depicts two realizations of an equal amplitude 10-tone multisine - one with constant phase distribution, and another with randomized phases - clearly shows that the amplitude distribution in time, or the peak power to average power ratio, is extremely different. This is of primordial importance to design validation, because not only the high peaks of Fig. 11 b) can drive the circuit into states whose corresponding nonlinear performance is totally altered, as it is known that various wireless standards may present very distinct peak power to average power ratios. That is illustrated in figure Fig. 12 a) and b) where frequency-domain power spectral density functions and time-domain waveforms of a GSM [48] and a WCDMA 2000 [49] signal are shown.

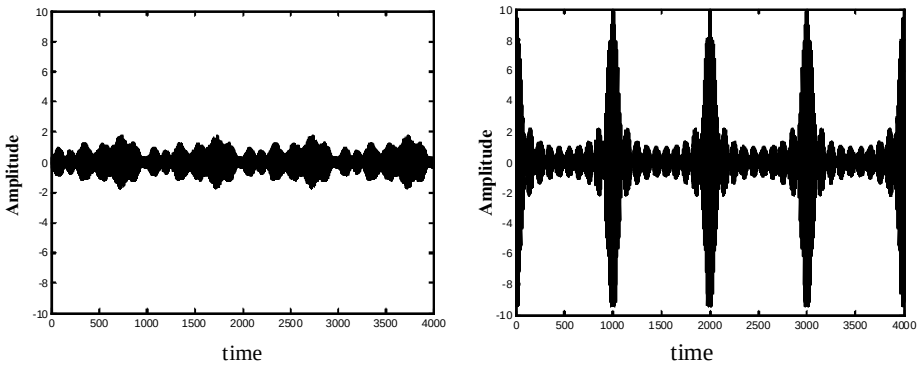

a) b)

Fig. 11 – Time waveforms of two multisines composed of 10 evenly spaced and equal amplitude tones, but with different phase arrangements. a) – Randomized phases. b) – Constant phases.

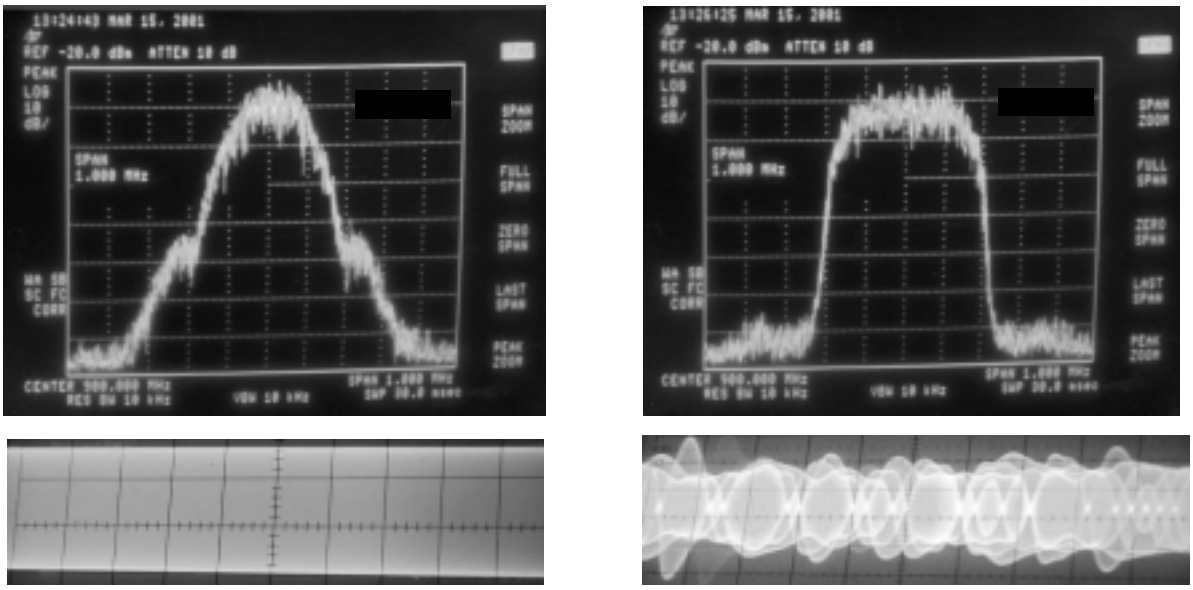

a) b)

Fig. 12 – Illustration of frequency-domain power spectral density functions (above) and time-domain waveforms (below) of a GSM – a) and a WCDMA 2000 – b) signal.

Turning now our attention to the design validation of general purpose circuits, the excitation signal can be chosen more freely, and so CW, two-tones and multi-tones tests are common.

From these options, the CW excitation is the one leading to the simplest laboratory set-ups [11], which also corresponds to easiest to set in HB harmonic-Newton simulators. Typical CW tests include output power (or gain) and phase measurements for input power sweeps, the so-called AM-AM and AM-PM tests in band-pass telecommunication systems [1,11].

Despite their simplicity, CW stimuli are being replaced by two-tone or multi-tone signals because of their recognized amplitude limitations and the impossibility to evaluate higher order memory. Indeed, being single frequency signals with constant envelope, they can not excite any base-band frequency component nor any amplitude state beyond the [-*A*, *A*] interval (where *A* is the CW RF signal amplitude).

One possible alternative to overcome these deficiencies is to use a two-tone signal [11]. As shown in Fig. 13 a), its envelope is no longer a constant but a sinusoid, and it already involves a non-null base-band frequency.

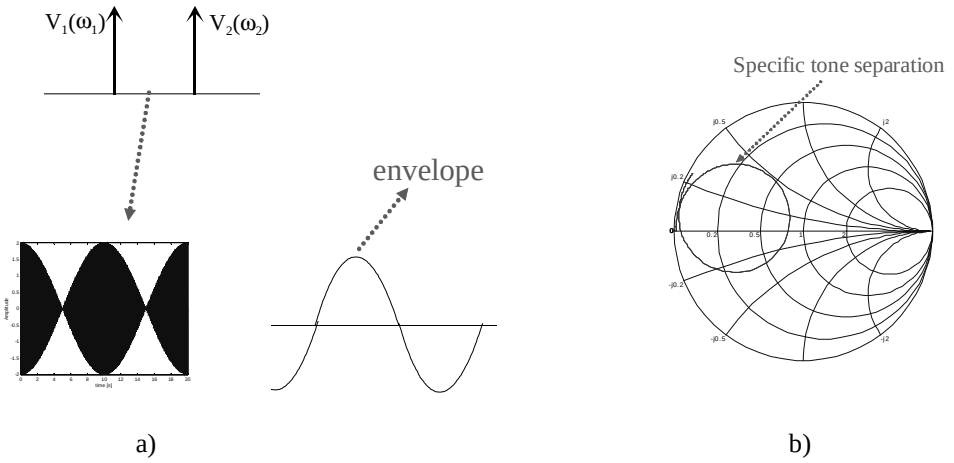

Fig. 13 – Two-tone stimulus for nonlinear memory testing. a) – RF signal and corresponding envelope waveforms. b) – Example of load impedance termination for a swept envelope frequency (two-tone separation).

As is depicted in Fig. 13 b), changing two-tone separation allows the exploration of the circuit's base-band behavior, although at a single frequency point for each experiment. So, this excitation can validate the design against several nonlinear effects as in-band intermodulation distortion, revealing some important long-term memory aspects like frequency separation dependent distortion or even IMD asymmetric behaviors [29, 30, 31, 32, 50]. This is illustrated in figure Fig. 14 where the observation of IMD asymmetries in our amplifier under test is a direct function of the envelope frequency which could then be related to the base-band load impedance shown in Fig. 13 b).

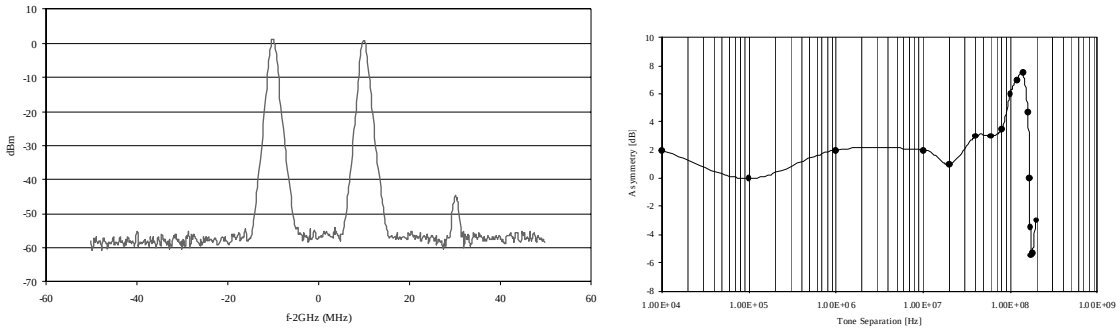

a) b)

Fig. 14 – Nonlinear two-tone IMD asymmetries as a manifestation of the circuit's envelope dynamics. a) – Typical observation of asymmetric IMD output spectrum when the envelope frequency was 120 MHz. b) – Variation of IMD asymmetry versus envelope frequency.

Finally, a tow-tone amplitude sweep can also reveal deeps or valleys in the IMD versus input power characteristics, which have been extensively used in the design of highly efficient and linear wireless power amplifiers. Fig. 15 is exactly an illustration and such measured and simulated results obtained with our example medium power amplifier.

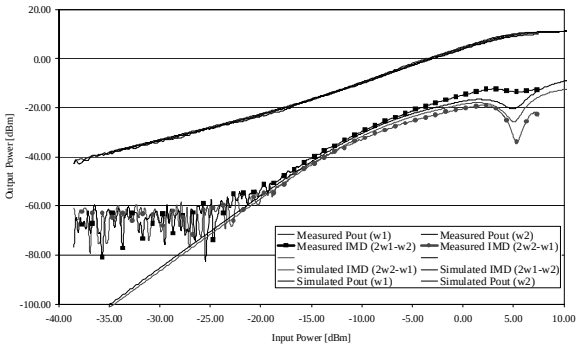

Fig. 15 – Results of measured and simulated two-tone IMD sideband amplitudes for an input power sweep.

Despite the base-band terminations are already being sensed in a two-tone test, no mixing products between different base-band components are still possible. Furthermore, this type of stimulus confines the input amplitude distribution to the [-2*A*, 2*A*] range, where *A* is again the amplitude of each tone.

Extending this stimulus for simultaneous multiple frequency beats and broader amplitude distribution requires excitations composed of multi-tones and of wider amplitude distribution in time. This implies an increase on the number of tones of a multisine (finer frequency resolution) but of randomized phases to obviate the odd amplitude distribution shown if Fig. 11 b). In the limit, when the number of tones tends to infinity and the phases are uniformly distributed over [0, 2π], the excitation tends to band-limited white Gaussian noise [36, 51]. This empirical model validation conclusion was already predicted by the Volterra-Wiener theories which showed that a white (or band-limited) Gaussian noise can, indeed, test a causal, stable system of finite memory span for all its nonlinear states and memory effects [16, 40].

So, general purpose circuits are more often tested under noise excitations, from which the measurements of noise power ratio [11], or of co-channel and adjacent-channel distortion [11] shown in Fig. 16, are just two widely spread examples.

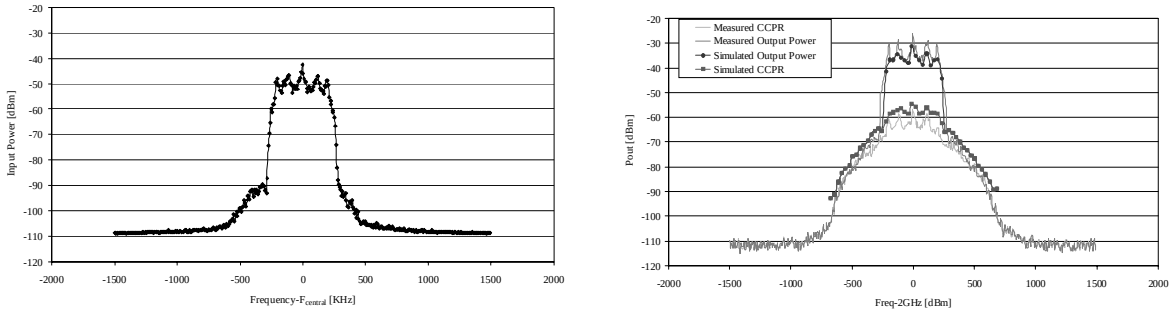

a) b)

Fig. 16 – a) Band-limited white Gaussian noise excitation used for the amplifier design validation. b) - Measurement and simulated results of co-channel and adjacent-channel distortion when the amplifier under test was subject to band-limited Gaussian noise. Simulated results were obtained with a multi-tone HB engine by averaging the model responses to a set of random multisine realizations.

Unfortunately, noise excitations are difficult to handle in practice, and, due to their true stochastic nature, impossible to simulate. So, the approximating alternative has been to rely on its (supposed) ergodicity, estimating their expected statistical properties (as power spectral density functions) from the

average of results taken from multisines of constant amplitude and randomized phase – random multisines – or of both random amplitude and phase – periodic noise - [36]. Fortunately, a series of recent mathematical results have shown that the response of a nonlinear dynamic system to a random multisine or periodic noise converges, under some weak restrictions, to the response to true Gaussian noise when the number of averaged realizations tends to infinity [36]. This provided HB multi-tone simulators based on the multi-dimensional Fourier transform [4] on spectral balance [52] or even on artificial frequency mapping techniques [53-55] with the necessary theoretical support to handle these more involved stochastic excitations. It was actually an HB engine based on an artificial frequency mapping that was used to compare the measurement results obtained with band-limited Gaussian noise with the simulated ones presented in Fig. 16 [11].

V. CONCLUSIONS

Although nonlinear network design is a problem of complex nature, it is rapidly advancing towards a mature state.

Because both short-term and long-term memory effects are involved, simulating nonlinear networks subject to telecommunication signals may require a wide variety of simulation tools as recently proposed mixed-mode multi-rate techniques. But, it also requires specific electron device and terminating networks modeling. That should be valid, not only near the excitation frequency, as at least the base-band and the first few harmonics of the RF signal.

As the response of a nonlinear network to a certain input can not be determined from the response to any other excitation, a conservative rule would say that it should be tested with signals as close as possible to the expected real ones. However, recent advances in system identification and nonlinear measurement science have shown that reasonable design analysis and validation can already be obtained from band-limited Gaussian noise or even averaged random multisine approximations.

ACKNOWLEDGEMENT

The authors would like to acknowledge the financial support provided by Portuguese Science Bureau, F.C.T., and the FEDER program under Project POCTI/ESE/37531/2002 – OPAMS.

REFERENCES

[1] M., Jeruchim, P. Balaban and K. Shanmugan, Simulation of Communication Systems, Boston: Kluwer Academic Publishers, (2nd Ed.), (2000).

[2] V. Rizzoli and A. Neri, State of the Art and Present Trends in Nonlinear Microwave CAD Techniques, IEEE Trans on Microwave Theory and Techniques, MTT-36 (1988), 343-365.

[3] M. S. Nakhla and J. Vlach, A Piecewise Harmonic Balance Technique for Determination of Periodic Response of Nonlinear Systems, IEEE Trans on Circuits and Systems, CAS-23 (1976), 85-91.

[4] V. Rizzoli, C. Cecchetti and A. Lipparni, A General-Purpose Program for the Analysis of Nonlinear Microwave Circuits Under Multitone Excitation by Multidimensional Fourier Transform, Proc. 17th European Microwave Conference, Rome (1987), 635-340.

[5] J. Roychowdhury, Analysing Circuits with Widely Separated Time Scales Using Numerical PDE Methods, IEEE Trans on Circuits and Systems - I, CAS-48 (2001), 578-594.

[6] K. Kundert, J. White and A. Sangiovanni-Vicentelli, Steady-State Methods for Simulating Analog and Microwave Circuits, Norwell, MA, Kluwer Academic Pub. (1990).

[7] E. Ngoya and R. Larchevèque, Envelop Transient Analysis: A New Method for the Transient and Steady State Analysis of Microwave Communication Circuits and Systems, Proc. IEEE Microwave Theory and Techniques Symposium Digest, California (1996), 1365-1368.

[8] V. Rizzoli, A. Neri and F. Mastri, A Modulation-oriented Piecewise Harmonic Balance Technique Suitable for Transient Analysis and Digitally Modulated Analysis, Proc. 26th European Microwave Conference, Prague, Cheks Rep. (1996), 546-550.

[9] J. C. Pedro and N. B. Carvalho, Simulation of RF Circuits Driven by Modulated Signals Without Bandwidth Constraints, 2002 IEEE International Microwave Theory and Tech. Symposium, Seattle, Jun. (2002).

[10] D. Sharrit, New Method of Analysis of Communication Systems, MTT-S Nonlinear CAD Workshop, Jun. (1996).

[11] José Carlos Pedro and Nuno Borges de Carvalho, Intermodulation Distortion in Microwave and Wireless Circuits, Norwood, Artech House (2003).

[12] L. W. Nagel, Spice2: A computer program to simulate semiconductor circuits, Electronic Research Laboratory, University of California-Berkeley, Memo ERL-M520 (1975).

[13] Simulink 5.0, The Mathworks, Inc. (2002).

[14] T. J. Aprille and T. N. Trick, Steady-State Analysis of Nonlinear Circuits With Periodic Inputs, Proceedings of the IEEE, Vol. 60 (1972), 108-114.

[15] S. A. Maas, Nonlinear Microwave Circuits, Norwood, MA, Artech House (1988).

[16] M. Schetzen, The Volterra and Wiener Theories of Nonlinear Systems, New York, John Wiley & Sons (1980).

[17] L.Chua and C. Ng, Frequency-domain analysis of nonlinear systems: formulation of transfer functions, Electronic Circuits & Systems, Vol. 6 (1979), 257-269.

[18] V. Rizzoli, F. Mastri, E. Furini and A. Costanzo, A Krylov-Subspace Technique For The Global Stability Analysis Of Large Nonlinear Microwave Circuits, IEEE MTT-S International, Vol. 1, May (2001), 435 -438.

[19] N. B. Carvalho and J. C. Pedro, Large and Small Signal IMD Behavior of Microwave Power Amplifiers, IEEE Trans on Microwave Theory and Techniques, MTT-47 (1999), 2364-2374.

[20] J.A. Garcia, J. C. Pedro, M. L. De la Fuente, N. B. Carvalho, A. Mediavilla, A. Tazon, Resistive FET Mixer Conversion Loss And IMD Optimization By Selective Drain Bias, IEEE MTT-S International, Vol. 2, June (1999) 803 -806.

[21] V. Rizzoli, A. Costanzo, A. Neri, A Novel Substitution Algorithm For The Efficient Analysis And Optimisation Of Microwave Oscillators, 27th European Microwave Week, Vol. 2 (1997), 826 -831.

[22] Y. Saad and M.H. Schultz, GMRES: A generalized minimal residual method for solving nonsymmetric linear systems, SIAM Journal Sci. Stat. Comput., 7 (1986), 856-869.

[23] H. Brachtendorf, G. Welsch, R. Laur and A. Bunse-Gerstner, Numerical Steady-State Analysis of Electronic Circuits Driven By Multi-Tone Signals, Electrical Engineering, 79 (1996), 103-112.

[24] P. Antognetti and G. Massobrio, Semiconductor Device Modeling with SPICE, London, McGraw-Hill International Editions (1988).

[25] I. Getreu, Modeling the Bipolar Transistor, New York, Elsevier (1976).

[26] J. Pedro and J. Perez, Accurate Simulation of GaAs MESFET's Intermodulation Distortion Using a New Drain-Source Current Model, IEEE Trans on Microwave Theory and Techniques, MTT-42 (1994), 25-33.

[27] Y. Cheng and C. Hu, Mosfet Modeling & BSIM3 Users's Guide, Boston, Kluwer Academic Publishers (1999).

[28] J. Pedro, J. C. Madaleno and J. A. Garcia, Theoretical Basis for the Extraction of Mildly Nonlinear Behavioral Models, International Journal of RF and Microwave Computer-Aided Engineering, Vol. 13, (2003), 40-53.

[29] W. Bosch and G. Gatti, Measurement and Simulation of Memory Effects in Predistortion Linearizers, IEEE Trans on Microwave Theory and Techniques, MTT-37 (1989), 1885-1890.

[30] N. B. Carvalho and J. C. Pedro, A Comprehensive Explanation of Distortion Sideband Asymmetries, IEEE Trans on Microwave Theory and Tech., MTT-50 (2002), 2090-2101.

[31] H. Ku, M. Mckinley and J. Kenney, Extraction Of Accurate Behavioral Models For Power Amplifiers With Memory Effects Using Two-Tone Measurements, IEEE MTT-S Int. Microwave Symp. Dig., Seattle, June (2002), 139-142.

[32] J.H.K. Vuolevi, T. Rahkonen and J.P.A. Manninen, Measurement Technique For Characterizing Memory Effects In RF Power Amplifiers, IEEE Trans on Microwave Theory and Techniques, MTT-49 (2001), 1383 -1389.

[33] S. Boyd, Ys Tang, Chua Lo, Measuring Volterra Kernels, IEEE T Circuits Syst CAS-30 (1983), 571-577.

[34] Chua Lo and Liao Yl, Measuring Volterra Kernels 2, Int J Circ Theor App 17 (1989), 151-190.

[35] Chua Lo, Liao Yl, Measuring Volterra Kernels 3, Int J Circ Theor App 19 (1991), 189-209.

[36] Rik Pintelon and Johan Schoukens, System Identification – A frequency domain approach, Piscataway ,IEEE Press, (2001).

[37] J. Schoukens, Y. Rolain and P. Guillaume, Design of narrowband, high-resolution multisines, IEEE Trans on Instrumentation and Measurement, IM-45 (1996), 750 -753.

[38] Kate Remley, Multisine Excitation for ACPR Measurements, IEEE MTT-S Int. Microwave Symp. Dig., Philadelphia, June (2003).

[39] Tianhai Wang and T.J. Brazil, Volterra-mapping-based behavioral modeling of nonlinear circuits and systems for high frequencies, IEEE Trans on Microwave Theory and Techniques, MTT-51 (2003), 1433 - 1440.

[40] V. John Mathews and Giovanni L. Sicuranza, Polynomial Signal Processing, Wiley-Interscience, (2000).

[41] C. P. Silva, Time-domain measurement and modeling techniques for wideband communication components and systems, International Journal of RF And Microwave Computer-Aided Engineering, 13 (2003), 5-31.

[42] G. Dambrine, A. Cappy, F. Heliodore and E. Playez, A New Method for Determining the FET Small-Signal Equivalent Circuit, IEEE Trans on Microwave Theory and Techniques, MTT-36 (1988), 1151-1159.

[43] J. C. Pedro, Physics Based MESFET Empirical Model, Proc. IEEE MTT-S International Microwave Symposium Digest, San Diego (1994), 973-976.

[44] J.C. Pedro, Evaluation of MESFET Nonlinear Intermodulation Distortion Reduction by Channel-Doping Control, IEEE Trans. on Microwave Theory and Techniques, MTT-45 (1997), 1989-1997.

[45] J. A. Garcia, A. Mediavilla, J. C. Pedro, N. B. Carvalho, A. Tazón and J. L. Garcia, Characterizing the Gate to Source Nonlinear Capacitor Role on GaAs FET IMD Performance, IEEE Trans on Microwave Theory and Techniques, MTT-46 (1998), 2344-2355.

[46] Visual System Simulator, Applied Wave Research, Inc. (2002).

[47] Advanced Design System 2002, Agilent Technologies, (2002).

[48] T. S. Rappaport, Wireless Communications - Principles and Practice, London, Prentice Hall (1996).

[49] V. Aparin, Analysis of CDMA signal spectral regrowth and waveform quality, IEEE Trans on Microwave Theory and Tech., MTT-49 (2001), 2306-2314.

[50] J. Wood and D. Root, The Behavioral Modeling of Microwave/RF ICs using Non-Linear Time Series Analysis, IEEE MTT-S Int. Microwave Symp. Dig., Philadelphia, June (2003).

[51] J. C. Pedro and N. B. Carvalho, On the Use of Multi-Tone Techniques for Assessing RF Components' Intermodulation Distortion, IEEE Trans on Microwave Theory and Techniques, MTT-47, (1999), 2393-2402.

[52] N. B. Carvalho and J.C: Pedro, Multi-tone Frequency Domain Simulation of Nonlinear Circuits in Large and Small Signal Regimes, IEEE Trans on Microwave Theory and Techniques, MTT-46 (1999), 2016-2024.

[53] D. Hente and R.H. Jansen, Frequency Domain continuation method for the analysis and stability investigation of nonlinear microwave circuits, IEE Proceedings-H Microwaves Antennas and Propagation, Vol. 133 (1986), 351-362.

[54] P. J. Rodrigues, Computer Aided Analysis of Nonlinear Microwave Circuits, Norwood, MA, Artech House (1998).

[55] J. C. Pedro and N.B. Carvalho, Efficient Harmonic Balance Computation of Microwave Circuits' Response to Multi-Tone Spectra, Proc. 29th European Microwave Conference, Munchen, (1999), 103-106.